International Communications in Heat and Mass Transfer 162 (2025) 108582

Contents lists available at ScienceDirect

International Communications in Heat and Mass Transfer

journal homepage: www.elsevier.com/locate/ichmt

Coupling effect in compacted panels based on micronized nanocellular polymers: Modeling of the thermal conductivity

Ismael Sánchez-Calderón [a,b], Félix Lizalde-Arroyo [a,*], Judith Martín-de-León [a], Miguel Ángel Rodríguez-Pérez [a,c], Victoria Bernardo [b]

[a] CellMat Laboratory, Campus Miguel Delibes, Faculty of Science, Condensed Matter Physics Department. University of Valladolid, Paseo de Belén 7, 47011 Valladolid, Spain
[b] CellMat Technologies S.L., Paseo de Belén 9-A, 47011, Valladolid, Spain
[c] BioEcoUVA Research Institute on Bioeconomy, University of Valladolid, 47011 Valladolid, Spain

ARTICLE INFO

Keywords:
Thermal conductivity
Poly(methyl-methacrylate)
Thermal insulation
Compacted micronized nanocellular polymer
Coupling effect

ABSTRACT

Compacted panels based on micronized nanocellular polymers show reduced thermal conductivity in comparison with bulk nanocellular polymers, especially under vacuum, so they are promising materials to be used as vacuum insulation panels (VIP). The discontinuous structure formed by micrometric particles allows for decreasing the conduction through the solid phase since the contact points between the particles act as additional thermal resistances to the heat transmission. However, the discontinuous structure also leads to the appearance of the coupling effect, which cannot be modeled using the typical equations for cellular polymers. In this work, a semi-empirical model able to predict the thermal conductivity of compacted panels based on nanocellular poly (methyl-methacrylate) (PMMA) is developed. The model allows quantifying each heat transfer mechanism contribution (conduction through the solid phase, conduction through the gas phase, radiation, and coupling effect). The model shows that the contribution of the coupling effect in the compacted panels is higher than 50 % of the total thermal conductivity for pressures higher than 5 mbar, supporting the need for the model to correctly predict the insulation performance of these materials. The model predicts minimum thermal conductivities of 32.5 mW/(m·K) at ambient pressure and of 10 mW/(m·K) at maximum vacuum.

1. Introduction

Vacuum insulation panels (VIPs) are one of the most promising high-performance thermal insulation materials [1], exhibiting thermal conductivities between 4 and 8 mW/(m·K) [2–5]. They can be described as an evacuated open porous material (core) placed inside a gas barrier envelope. The materials usually selected as core materials are based on fumed/precipitated silica, silica aerogel, glass fibers, and open cell rigid polyurethane foams (PUR) [6]. The physics behind their super-thermal insulation behavior are well-known [1,7–11]: the total thermal conductivity (λ_t) can be described as a sum of five heat transfer mechanisms (Eq. (1)): conduction through the solid phase (λ_s), conduction through the gas phase (λ_g), radiation (λ_r), convection (λ_c), and coupling (λ_{coup}) [12–18]. From these contributions, convection can be neglected [19–21]. For instance, Jeffreys [22] showed that cellular materials with cells of 1 mm lack convective flow. Thus, when the core is fully evacuated, the conduction through the gas phase and the coupling contribution became null leading to a drastic decrease in the thermal conductivity.

$$\lambda_t = \lambda_s + \lambda_g + \lambda_r + \lambda_c + \lambda_{coup} \quad (1)$$

The coupling term takes into account the interaction between the core particles and the gas [1,7], so it is important for particle-based materials (such as fumed silica) but negligible for materials with continuous structure [1,10,16,17]. As previously commented, at the normal operating conditions of VIPs (vacuum) it becomes null due to the lack of gas molecules, but at ambient pressure, it can have a significant contribution to the total thermal conductivity [8,10,11,23]. For instance, Fricke et al. [10] reported coupling contributions between 20 and 30 mW/(m·K) for powders consisting of hard grains (perlite and diatomite), leading to a higher thermal conductivity than expected at ambient pressure. Similar behavior was observed by Reichenauer et al. [9] and by Swimm et al. [23] for a system consisting of solid glass spheres of 1 mm diameter and for an organic aerogel (pore size of 600

* Corresponding author.
E-mail address: felix.lizalde@uva.es (F. Lizalde-Arroyo).

https://doi.org/10.1016/j.icheatmasstransfer.2025.108582

Available online 10 January 2025

nm), respectively. However, despite the importance of the coupling effect, only a few authors modeled the coupling due to its complexity. Swimm et al. [24], Zhao et al. [25], and Bi et al. [26] modeled analytically the coupling effect for aerogels. Meanwhile, Verma et al. [27] and Liu et al. [28] developed a numerical model which already takes into account the coupling for perlite-based systems and aerogels, respectively. On the other hand, Swimm et al. [17,23] and Sonnick et al. [16] modeled semi-empirically the coupling for aerogels and precipitated silica, respectively. They show that the coupling depends on the density (the higher density, the higher coupling) [16,23].

In our previous work [29], we produced vacuum insulation panels based on micronized nanocellular poly(methyl-methacrylate) (PMMA) with densities ranging from 160 and 360 kg/m^{3,} and cell sizes between 400 and 4000 nm, thermal conductivities between 37 and 51 mW/(m·K) at ambient pressure, and thermal conductivities ranging from 11 to 18 mW/(m·K) at vacuum (0.02 mbar). This was the first time such material was produced and characterized. The thermal conductivity results at ambient pressure and under vacuum provided surprising results, obtaining higher thermal conductivity reductions when vacuuming than expected, and this behavior was attributed to the coupling effect. The thermal conductivity of bulk nanocellular polymers, characterized by a continuous structure, has been modeled extensively in the past [15,30–36]. However, none of the previous models allowed to predict how nanocellular polymers would behave after micronization. Micronized nanocellular polymers are novel materials, characterized by a discontinous structure with the nanocells inside the micrometric particles [37]. Micronized nanocellular polymers rise as an attempt to enhance the thermal insulation behavior of nanocellular polymers [29,37], which present high conduction through the solid phase and radiation as shown by recent theoretical and experimental works [15,32–34]. Therefore, the modeling of the thermal conductivity of micronized nanocellular polymers is of utmost importance to continue exploring this novel route, since the compacted panels based on micronized microcellular and nanocellular polymers potential candidates to be used as alternative low-cost and environmentally friendly materials for VIP productions.

In this work, a semi-empirical model to predict the thermal conductivity of compacted panels based on micronized nanocellular PMMA that only depends on the material characteristics (density, cell size, and particle size) and the measurement conditions (pressure and temperature) is developed. For the first time, the coupling effect is studied in micronized nanocellular polymer systems. Results show that these materials are quite promising for VIP applications since under vacuum it is possible to achieve quite low thermal conductivities, below those obtained with bulk nanocellular polymers.

2. Experimental

VIPs based on compacted panels of dimensions of 120 × 120 × 15 mm^3 were produced from microcellular and nanocellular micronized PMMA (Fig. 1). Details about the production of the bulk microcellular and nanocellular PMMA via gas dissolution foaming using CO_2 as a blowing agent, the micronization process using a rotor beater mill, the compaction process using a hot press, the VIP fabrication process, and the characterization of these samples can be found in our previous works [15,29,37]. The PMMA grade used was PLEXIGLAS® 7H kindly supplied by Röhm GmbH. This PMMA presents a density of 1190 kg/m^3, a melt flow index of 0.77 g/10 min (measured at 230 °C and 2.16 kg), and a glass transition temperature of 110.4 °C measured by DSC (model DSC3+, Mettler).

Table 1 gathers the main features of the compacted samples which are going to be used to develop the semi-empirical model to predict their thermal conductivity. Apparent density (ρ_{app}) was obtained according to UNE-EN 1602 [29,38]. Cell size (ϕ_{3D}) was obtained after analyzing the cellular structure from scanning electron microscopy (SEM) micrographs [15,39]. Particle size (D) was obtained through image analysis [37,40]. Open cell content (OC) was measured according to ISO 4590 [37,41]. Thermal conductivity under maximum vacuum (0.02 mbar) (λ_{vacuum}) at 10 °C and thermal conductivities at ambient pressure ($\lambda_{ambient\ pressure}$) at different temperatures (10, 20, 30, and 40 °C) were measured using a thermal heat flow meter model FOX 200 (TA Instruments / LaserComp, Inc.), which measures according to ASTM C518 and ISO 8301 [42,43] (steady-state conditions) with an absolute accuracy of ±1 % [29]. The thermal temperature gradient was set to 20 °C (i.e., for the measurements at 10 °C, the temperature goes from 0 °C in the upper isothermal plate to 20 °C in the lower one). The measurement temperatures were selected according to the literature [15,44–46]. Measurements were also performed under different pressures (600, 300, 200, 100, 60, 30, 10, 6, and 3 mbar) at 10 °C and used to validate the model. For the measurements under vacuum, a set-up consisting of a vacuum pump (RV3, Edwards), a vacuum controller (VacuuSelect + VV-B15C electrovalve + Pirani VacuuWiew extend sensor, Vacuubrand), a vacuum valve (VAC VALVE 425, Matva), and a vacuum bag (Pack-lab) were used. See [29] for further details about the procedure of the vacuum measurements.

3. Model: experimental determination of the coupling effect

Fig. 2 shows a scheme of the different heat transfer mechanisms affecting a bulk material (Fig. 2a) and a compacted panel made of micrometric particles (Fig. 2b). In a bulk material, the main heat transfer mechanisms are conduction through the solid phase, conduction through the gas (cells) phase, and radiation. Meanwhile, in a compacted panel made of micrometric particles an additional mechanism, the coupling effect, emerges due to the discontinuous structure. Also, the discontinuous structure affects the conduction mechanisms. Therefore, the proposed semi-empirical model:

- Is based on calculating the contributions of the different heat transfer mechanisms as presented in Eq. (1).

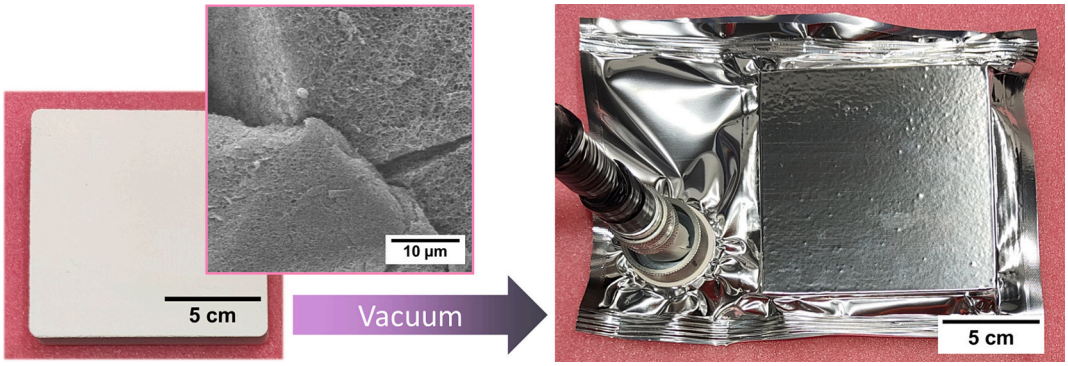

Fig. 1. Picture of the compacted panel picture, its correspondent VIP, and SEM micrograph of its structure.

Table 1
Density, cell size, particle size, open cell content, thermal conductivity under vacuum (0.02 mbar) and 10 °C, and thermal conductivity at ambient pressure at different temperatures (10, 20, 30, and 40 °C) of the compacted panels.

Sample	ρ_{app} (kg/m^3)	ϕ_{3D} (nm)	SD/ϕ_{3D_B}	D (μm)	SD/D	OC (%)	λ_{vacuum} (mW/(m·K))	$\lambda_{ambient\ pressure}$ (mW/(m·K))			
							10 °C	10 °C	20 °C	30 °C	40 °C
C1	158	1459	0.41	77	0.68	87 ± 1	11.6	36.6	37.5	38.4	39.2
C2	223	3215	0.70	92	0.73	98 ± 1	10.7	41.1	41.9	42.8	43.7
C3	292	1021	0.45	109	0.68	85 ± 1	16.7	44.6	45.4	46.3	47.0
C4	190	2916	0.59	102	0.78	94 ± 1	11.2	38.8	39.8	40.7	41.6
C5	201	468	0.47	94	0.62	98 ± 1	12.9	38.0	38.7	39.5	40.3
C6	357	2379	0.65	139	0.64	80 ± 1	18.1	51.1	52.0	52.9	53.8
C7	265	408	0.47	102	0.64	92 ± 1	16.5	42.2	42.9	43.7	44.4
C8	282	394	0.43	100	0.69	97 ± 1	18.5	44.2	44.7	45.5	46.1

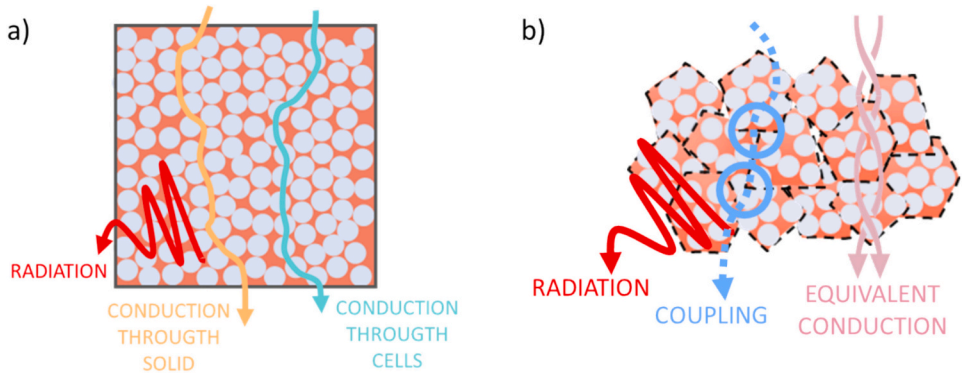

Fig. 2. Scheme of the heat transfer mechanisms in: a) bulk material and b) compacted paned made of micrometric particles.

- Presents the main novelty of calculating the conduction mechanisms considering a system of independent particles, as described below.
- Accounts for the coupling effect which is determined from the experimental data.
- Assumes that the radiation contribution of the compacted panels behaves similarly to bulk materials with the same density.
- Does not account for thermal bridging since it has not been observed in the experimental measurements.
- Depends only on the properties of the compacted material (apparent relative density, cell size, and particle size) and the measurement conditions (temperature and pressure), representing an advantage over numerical or theoretical models that require more parameters and assumptions being more difficult to use. Table 2 shows the constants and values that are going to be considered for the thermal conductivity modeling.

3.1. Conduction mechanisms: association of thermal resistances

On the one hand, the model is based on assuming an infinite series-parallel association of the powder particles to describe the conduction through the material. In conventional models for the conduction of porous material, the conduction term is calculated as a sum of the conduction through the solid (λ_s) and the conduction through the gas (cells) phase ($\lambda_{g,cells}$). In our system, we have a high number of independent particles, each of them characterized by its own conduction term ($\lambda_s + \lambda_{g,cells}$), in contact to one another. To calculate an equivalent conduction, we will assume each particle is acting as a thermal resistance, and that the collection of them can be modeled as an infinite association of thermal resistances in a series-parallel model. Then, using Ohm and Kirchhoff's law's, we can calculate the equivalent conduction though all the particles using Eq. (2). The term $(1+\sqrt{3})$ is obtained by applying Ohm and Kirchhoff law's (association of infinite resistances in series-parallel configuration [47]). It is important to remark that there are several works where the conduction of powdered systems is treated as an association of resistances [48–57], but as far as the authors know, this is the first time the hypothesis of assuming an infinite series-parallel association is used to describe the thermal conductivity.

$$\lambda_{eq} = \frac{\lambda_s + \lambda_{g,cells}}{1+\sqrt{3}} \tag{2}$$

The conduction through the solid phase of each particle (λ_s), depends on its solid volume fraction (X_s), the conductivity of the solid matrix (λ'_s), and a structural factor g (Eq. (3)). Note that for the porpose of the model, we are treating each particle as an individual bulk material, meaning that all the conduction information is gathered into the assumption of infinite series-parallel association of particles. Therefore, as we proved in our previous work where we modeled semi-empirically bulk micro-and nanocellular PMMA, the solid volume fraction (X_s) is the apparent relative density, defined as $\rho_{r,app} = \rho_{app} / \rho_s$, where ρ_{app} is the apparent density and ρ_s is the density of the solid PMMA (1190 kg/m^3); the conductivity of the solid PMMA (λ'_{s_PMMA}) depends on the temperature as shown in Table 2; and the g factor is considered to be 0.89 [15]. Nevertheless, since in the present work we are treating with a system consisting in powder particles, the effective g factor of the total compacted sample is going to be 0.33 (because of the dividing term in Eq. (2)). This value of g is very low in comparison with the value of the bulk material: therefore, this hypothesis implies that the conduction through the solid phase is very much reduced because of the presence of thermal resistances between the powder particles.

$$\lambda_s(mW/(m{\cdot}K)) = \lambda'_s g X_{s,powder} = \lambda'_{s\_PMMA} g_{PMMA} \rho_{r,app} \tag{3}$$

Meanwhile, the conduction through the cells of each particle ($\lambda_{g,cells}$) depends on the thermal conductivity of the gas ($\lambda'_{g,cells}$) and the cells volume fraction ($X_{g,cells}$) (that can be calculated as $1 - \rho_{r,app}$) (Eq. (4)). The conductivity of the gas is not that of the air, but it is reduced due to the Knudsen effect (Eq. (4)). The Knudsen effect equation is well-known and has been validated in several systems [18,58–60]. Therefore, the

Table 2
Constants and values used for the thermal conductivity model.

	Parameter		Value	Units
Variables	$\rho_{r,app}$	Apparent Relative Density	Variable for each material	–
	ϕ	Cell Size	Variable for each material	m
	D	Particle Size	Variable for each material	m
	T	Temperature	283.15 → 313.15	K
	p	Pressure	0.01 → 101,325	Pa
Parameters	λ'_{s_PMMA}	Solid PMMA Thermal Conductivity	0.2060 T + 115.5811	mW/(m·K)
	g	Solid Structure Factor	0.89	–
	λ'_{g0_air}	Air Thermal Conductivity	0.0741 T + 3.4029	mW/(m·K)
	d_m	N_2 Molecule Diameter	$3.6 \cdot 10^{10}$	m
	β	Energy Tranfer Parameter	1.64	–
	n	Micro-and nanocellular PMMA Refractive Index	1	–
	K_{e_PMMA}	Micro-and nanocellular PMMA Extintion Coefficent	$(5.6712 \cdot 10^6\ \phi^{0.4264})\ \rho_{r,app}$	m^{-1}
	A	Coupling f factor Slope	−0.0045 T + 3.0725	–
	B	Coupling f factor y-intercept	0.0006 T + 0.7133	–
Universal Constants	R	Ideal Gas Constant	8.31446	(Pa·m³)/(mol·K)
	N_A	Avogadro's Number	$6.022 \cdot 10^{23}$	molecules/mol
	σ	Stefan-Boltzmann constant	$5.67 \cdot 10^{-8}$	W/(m²·K⁴)

conductivity of the gas inside the cells is reduced as the cell size is reduced, and also when pressure is reduced by vacuuming. Thus, the conduction through the cells phase also depends on the conductivity of air (λ'_{g0_air}) (which is a function of the temperature as shown in Table 2 [61]), the cell size (ϕ), an intrinsic parameter that considers the transfer of energy between the gas molecules and the solid structure (β), the temperature (T), the pressure (p), the molecule diameter (d_m), the ideal gas constant (R) and the Avogadro's number (N_A). All the constants used for the model calculations are also collected in Table 2.

$$\lambda_{g,cells}(mW/(m{\cdot}K)) = \lambda'_{g,cells} X_{g,cells} = \frac{\lambda'_{g0\_air}(1-\rho_{r,app})}{1+\frac{2\beta}{\phi}\frac{RT}{\sqrt{2}\pi d_m^2 N_A p}} \quad (4)$$

3.2. Radiation

On the other hand, thermal radiation (λ_r) is supposed to follow the Rosseland equation (Eq. (5)) [62,63]. The radiation term depends on the temperature (T), the Stefan-Boltzmann constant (σ), the refractive index (n), and the extinction coefficient (K_e). We make the hypothesis that the presence of the particle interfaces does not create additional scattering surfaces for radiation, and we assume that the compacted powders behave similarly to bulk materials with the same density as far as the radiation contribution is concerned. Therefore, K_e can be calculated with an empirical equation obtained in a previous work for bulk micro-and nanocellular PMMA that takes into account the cell size (ϕ) and the relative apparent density ($\rho_{r,app}$) (Table 2) [15].

$$\lambda_r(mW/(m{\cdot}K)) = \frac{16n^2\sigma T^3}{3K_e}\cdot 1000 = \frac{16n^2\sigma T^3}{3K_{e\_PMMA}}\cdot 1000 \quad (5)$$

3.3. Coupling effect

There are some models to describe the coupling term (λ_{coup}). In the simplest case, as proposed by Swimm et al. [17], it can be described as a series connection of thermal resistances between the solid (R_s) and the gas (R_g) phases (Fig. 3). Using the general relation for a thermal resistance ($R = d / \lambda$, where R is the thermal resistance, d is the distance, and λ the thermal conductivity), the following equation (Eq. (6)) can be derived to describe the coupling. Where d_s and d_g are the thickness over which the heat is transferred within the solid and gas phases. The system is described in terms of a unit cell that contains all the information (the unit cell thickness is $d_{unit\ cell}$). In this model, all influencing parameters like the particle surface geometry near the area of particle-to-particle contact or the thermal conductivity of the solid are combined in one-factor f, which may be a function of the porosity of the material [16]. As the f factor is usually the only unknown parameter, it can be obtained by solving the overall thermal conductivity equation and fitting the calculated data to the experimental data using the method of the least squares [16,23]. For instance, Sonnick et al. [16] obtained that $f = -18.68V_f + 17.94$ (where V_f is the porosity, which range between 0.92 and 0.76) for a precipitated silica system. Therefore, f takes values from 0.75 to 3.74. Meanwhile, Swimm et al. [23] obtained f values of 1.73 to 2.25 for two organic aerogels of porosities of 0.78 and 0.76 respectively (if doing a linear fit, $f = -26.00\ V_f + 22.01$). Whereas Heinemann et al. [64] mentioned that for a bed of glass spheres f would be 7.

$$\lambda_{coup} = \frac{d_{unit\ cell}}{R_s + R_g} = \frac{d_s + d_g}{\frac{d_s}{\lambda_s} + \frac{d_g}{\lambda_g}} = \lambda_g \frac{\lambda_s(d_s + d_g)}{\lambda_g d_s + \lambda_s d_g} = \lambda_g \cdot f \quad (6)$$

Applying Eq. (6) to the powdered systems, the thermal conductivity of the gas is that of the air, which is described by the Knudsen effect, depending on the particle size (D) because the coupling effect is related to the presence of the particles [16]. So, the coupling effect is described by Eq. (7). All terms are known except the f factor.

$$\lambda_{coup}(mW/(m{\cdot}K)) = \frac{\lambda'_{g0\_air}}{1+\frac{2\beta}{D}\frac{RT}{\sqrt{2}\pi d_m^2 N_A p}}\cdot f \quad (7)$$

3.3.1. Determination of the f factor

The only unknown parameter to predict the thermal conductivity is the f factor. It is calculated for each compacted material at different temperatures by solving Eqs. (7) and (8):

$$\lambda_{coup} = \lambda_t - \lambda_{eq} - \lambda_r \quad (8)$$

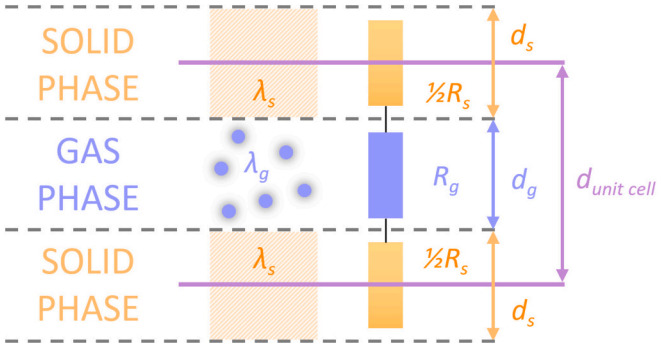

Fig. 3. Simple resistance model to describe the coupling of solid and gas heat conduction (adapted from [17]). The violet lines indicate one unit cell. (For interpretation of the references to colour in this figure legend, the reader is referred to the web version of this article.)

Where λ_t is the experimental thermal conductivity and λ_{eq} and λ_r are calculated based on Eqs. (2), (3), (4), and (5). Constants and values used for the calculations are gathered in Table 2. Then, the results of the experimental f factor at each temperature are fit as a function of the apparent relative density using the method of the last squares [16], as shown in Fig. 4a. For the samples produced in this work, f takes values from 0.75 to 1.09. Note that, the higher the f factor, the higher coupling (Eq. (7)). As density increases, the f factor increases (Fig. 4a) leading to a higher coupling contribution. It was observed that the fitting parameters were also a function of the temperature as shown in Fig. 4b. So, the f factor has been defined as a function of the apparent density and the temperature. As far as the authors know, this is the first time that f is defined also as a function of the temperature, but, looking at Eq. (6), since the thermal conductivity of the solid and gas depends on the temperature, it makes sense for f to be also a function of the temperature. As temperature increases, the f factor decreases (Fig. 4a) leading to a lower coupling contribution.

Table 3 summarizes the obtained parameters and correlation coefficient (r^2) in the first and second fitting (Fig. 4a and Fig. 4b in the manuscript respectively) for the calculus of the f factor. A is the slope and B is the y-intercept in the first fitting for each temperature (f factor as a function of the apparent relative density). Whereas A' is the slope and B' is the y-intercept in the second fitting (calculated parameters (slopes and y-intercepts) in the first fitting as a function of the temperature). It is observed that the correlation coefficient obtained on both adjustments is high (over 0.9).

Therefore, the total thermal conductivity (λ_t) of the compacted systems is described by Eq. (9). Note that this equation may be valid for compacted panels made by micronized micro-and nanocellular PMMA but also for other micronized cellular polymers or systems consisting of particles in contact. For different materials, the different inherent parameters (conduction of the solid, f factor, and extinction coefficient) should be determined to adjust the model to the characteristics of the new system.

$$\lambda_t(mW/(m\cdot K)) = \frac{\lambda'_{s\_PMMA} g_{PMMA} \rho_{r,app} + \frac{\lambda'_{g0\_air}(1-\rho_{r,app})}{1+\frac{2\beta}{\phi}\frac{RT}{\sqrt{2}\pi d_m^2 N_{Ap}}}}{1+\sqrt{3}} + \\ + \frac{16n^2\sigma T^3}{3K_{e\_PMMA}}\cdot 1000 + \frac{\lambda'_{g0\_air}}{1+\frac{2\beta}{D}\frac{RT}{\sqrt{2}\pi d_m^2 N_{Ap}}}\cdot(A\rho_{r,app}+B) \quad (9)$$

4. Model validation and predictions

4.1. Validation: comparison of the model predictions with the experimental results for the compacted panels

Fig. 5 shows the experimental thermal conductivity of the compacted samples C1 to C8 at 10 °C as a function of pressure and the predicted values given by the model according to Eq. (9). It is observed that the predicted thermal conductivity curve fits very well with the experimental data proving the validity of the model, as will be further discussed in the paragraphs. In addition, it is important to remark that the novel hypothesis of assuming an infinite series-parallel association for describing the conduction is the key to the model. For instance, at maximum vacuum (where the only heat transfer mechanisms are radiation and conduction through the solid phase) it allows predicting similar values to the experimental ones. But it also allows, together with the coupling, to predict similar values throgouth the vacuuming curve (Fig. 5h). However, some discrepancies, mostly under vacuum, are observed. One possible reason of these discrepancies can be related to the the use of the mean values of cell size and particle size for the calculations. Another possible reason is the open cell content. Since the materials are not 100 % open, they probably cannot be fully evacuated, resulting in a measurement under vacuum that will not correspond to an actual 0.02 mbar inner pressure.

In particular, Fig. 6 shows the experimental and predicted thermal conductivities of the compacted panel #5 at 10 °C as a representative example. It is observed that the prediction of our model adjusts well to the experimental points at different pressures. The thermal conductivity at 10 °C as a function of the pressure of bulk sample #5 and its prediction according to the equation obtained in [15] has also been included in Fig. 6 as a reference. While in the bulk material, there is only one drop of thermal conductivity (due to the Knudsen effect associated with the conduction through the gas phase), in the compacted sample there is a double drop: one due to the Knudsen effect affecting the conduction through the gas in the cells, and the other one due to the coupling effect. The drop due to the Knudsen effect affecting the conduction through the cells phase is governed by the cell size, meanwhile, the drop due to the coupling effect is governed by the particle size.

On the other hand, Fig. 7a and Fig. 7b show the predictions of the thermal conductivity of the compacted samples C1 to C8 according to Eq. (9) at ambient pressure and under maximum vacuum (0.02 mbar) respectively. Fig. 7a shows the results at ambient pressure and different temperatures (y axis) as a function of the experimental result for the same sample (x axis) according to the data of Table 1. It is observed that

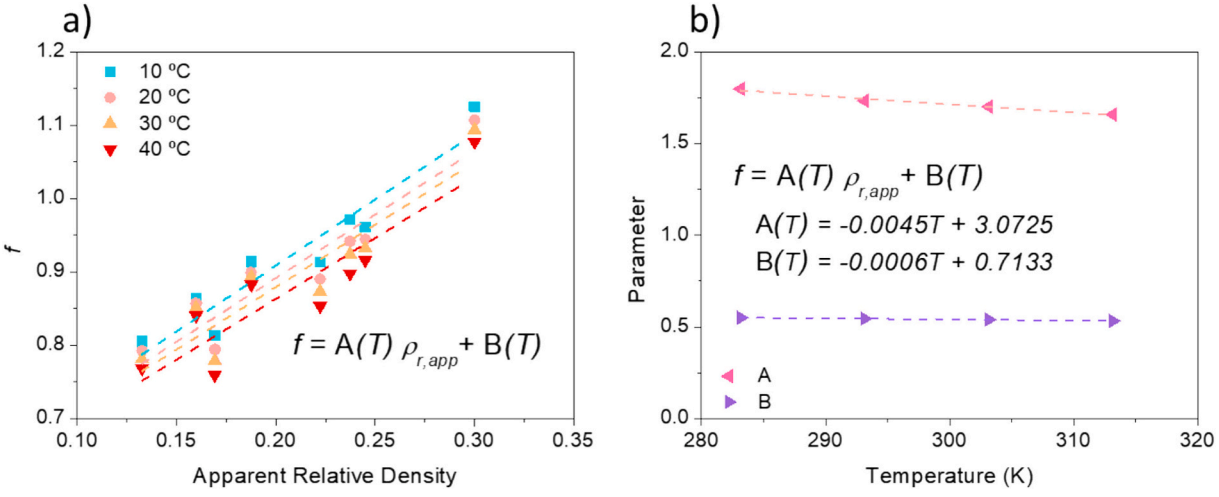

Fig. 4. Determination of the f factor: a) f as a function of the apparent relative density of the compacted samples for different temperatures, and b) fitting parameters as a function of the temperature.

Table 3
Obtained parameters and correlation coefficient (r^2) in the first and second fitting (Fig. 8**a** and **b** in the manuscript respectively) for the calculus of the *f* factor.

	FIRST FITTING				SECOND FITTING		
T (K)	*A*	*B*	r^2				
283.15	1.797545	0.5491	0.9529	Parameter	*A'*	*B'*	r^2
293.15	1.733235	0.5449	0.9380	*A(T)*	−0.0045	3.0725	0.9903
303.15	1.6998	0.5393	0.9247	*B(T)*	−0.0006	0.7133	0.9920
313.15	1.6577	0.5318	0.9073				

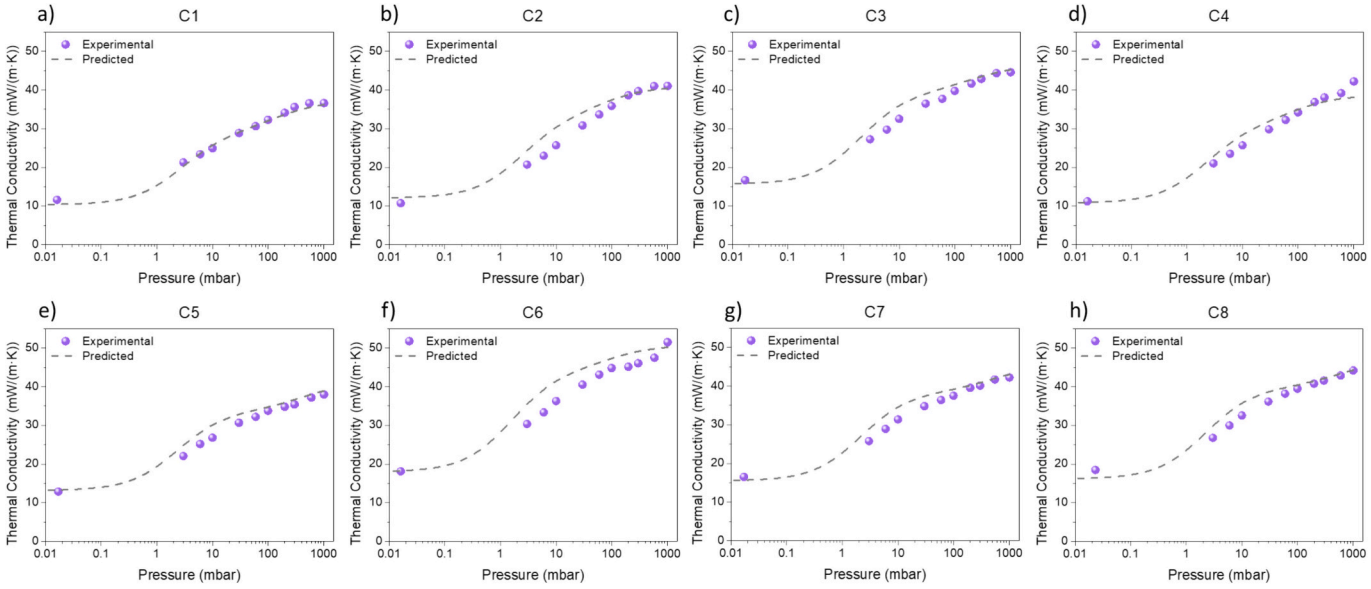

Fig. 5. Experimental thermal conductivity of the compacted samples at 10 °C and different pressures and prediction of the thermal conductivity as a function of pressure: a) C1, b) C2, c) C3, d) C4, e) C5, f) C6, g) C7, and h) C8.

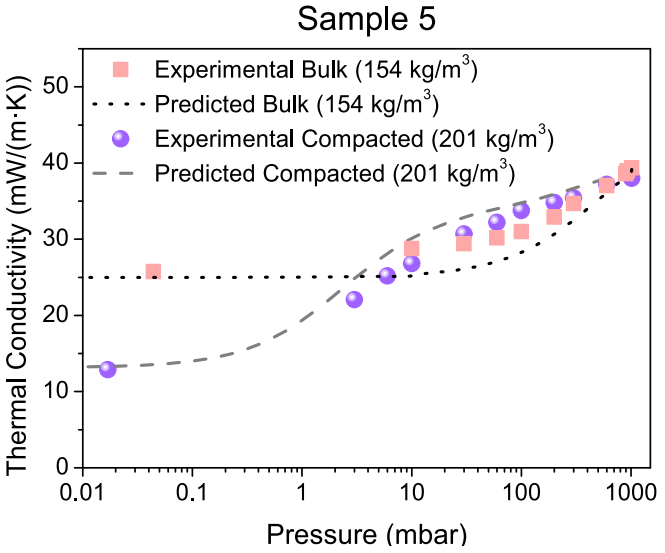

Fig. 6. Thermal conductivity at 10 °C as a function of the pressure of the compacted panel #5 and prediction according to Eq. (9). The thermal conductivity at 10 °C as a function of the pressure of bulk sample #5 and its prediction according to the equation obtained in [15] has been included as a reference.

there is a good correlation between the experimental values and the predicted ones since all the data points lie close to the theoretical line x = y that would correspond to perfect agreement between the data. Meanwhile, Fig. 7b shows the results of the model at 10 °C and at maximum vacuum (0.02 mbar) (y axis) compared to those obtained experimentally at the same conditions for each sample (x axis, data from Table 1). Again, good agreement is observed. The absolute differences are calculated in Fig. 7c and Fig. 7d. Regarding the predictions at ambient pressure the average absolute difference of the predictions at the different temperatures is lower than 0.8 mW/(m·K) (0.7 mW/(m·K) at 10 °C) (Fig. 7c). Therefore, the predicted values adjust well to the experimental measurements, with deviations below 3.5 %. At vacuum, the average absolute difference at 10 °C is lower than 1.0 mW/(m·K) (see Fig. 7d). As previously disccused, the discrepancies can be related to the open cell content and/or the use of the mean values of the different parameters for the calculations.

Fig. 8 shows the calculated thermal conductivities of the PMMA compacted panels at 10 °C and their contributions from conduction through the gas in the cells and the solid, radiation, and coupling in mW/(m·K) (Fig. 8a) and in % of the total thermal conductivity (Fig. 8b). It is observed that the coupling effect represents about 53 % (around 20 mW/(m·K)) of the total thermal conductivity, followed by the conduction through the solid phase (approximately 27 %), conduction through the cell phase (which ranges between 10 and 18 %), and radiation (which ranges between 2 and 9 %). Note that the radiation contribution of the nanocellular samples (C5, C7, and C8) is higher, and also C1 presents higher radiation, probably due to its low density. The conduction through the solid phase is quite low in comparison with a bulk nanocellular polymer [15] because the effective *g* factor in this material is 0.33 (2.7 times lower than that of bulk materials). The conduction of the gas inside the cells represents a small fraction of the total due to the assumption of the model of considering this mechanism an association of thermal resistance. Meanwhile, the high fraction represented by the coupling effect remarks the need of the proposed model to understand

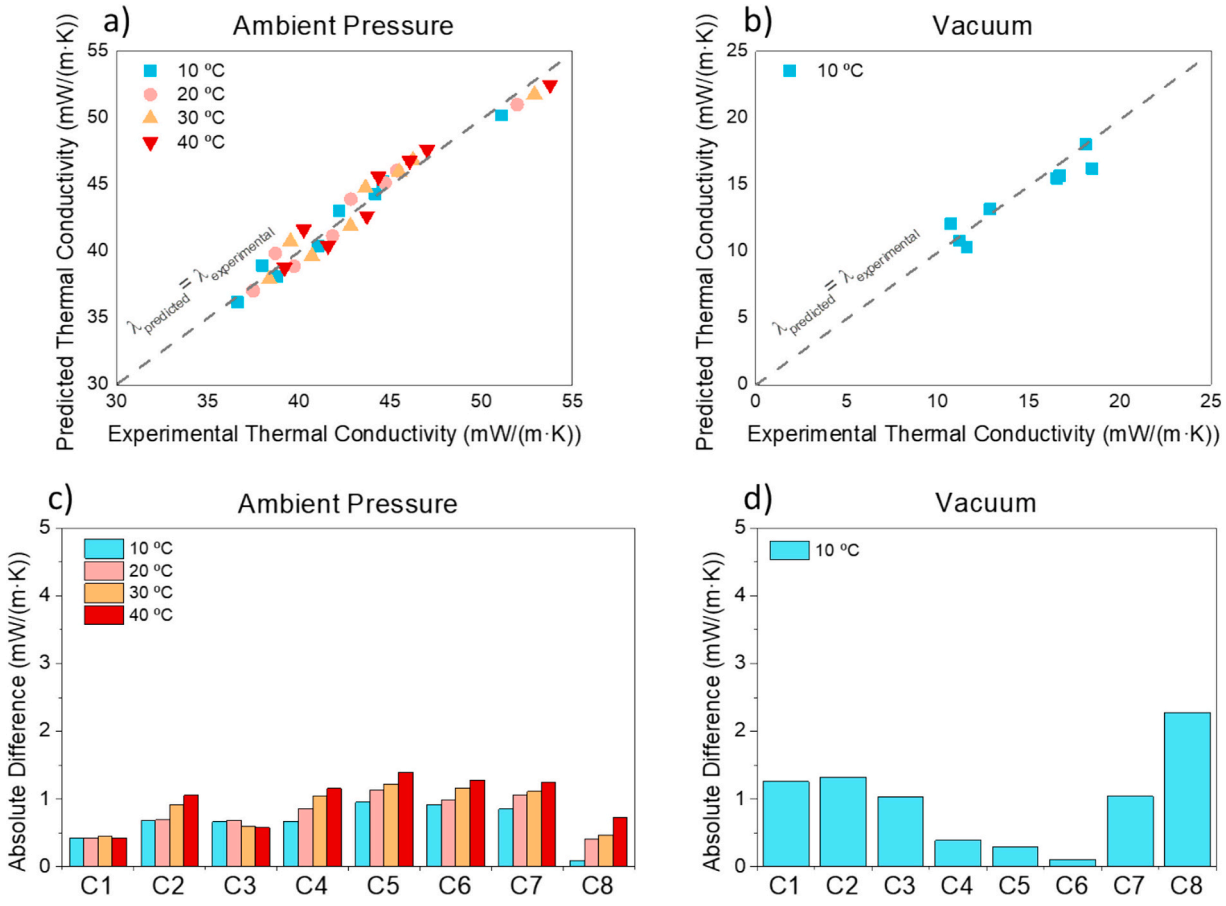

Fig. 7. Predicted vs experimental thermal conductivities of the compacted panels at various temperatures and ambient pressure (1013 mbar) (a), and at 10 °C and maximum vacuum (0.02 mbar) (b). Absolute differences of the predictions of the compacted samples at various temperatures and ambient pressure (a), and at 10 °C and maximum vacuum (0.02 mbar) (b). The dotted lines of a) and b) represent a line of x = y, that is, a theoretical line in which the predicted and experimental values would perfectly fit, used solely as a visual reference.

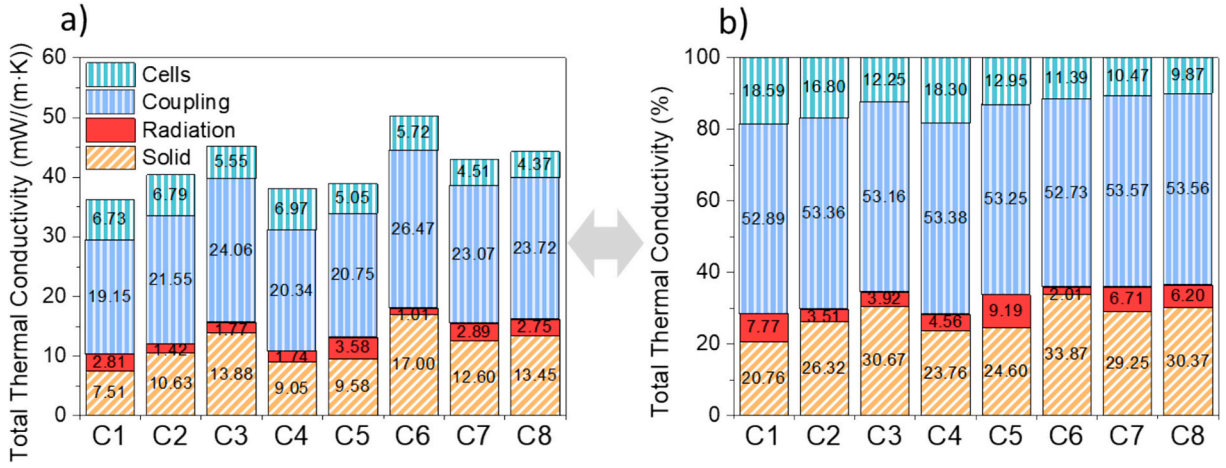

Fig. 8. Predicted contribution of each heat transfer mechanism to the total thermal conductivity of the compacted panels at 10 °C in mW/(m·K) (a) and in % of the total thermal conductivity (b).

the thermal conductivity of the micronized nanocellular materials: their behavior cannot be understood without this additional heat transfer mechanism. The coupling effect represents the same fraction in all the materials, regardless the size of the cells and even the density.

Therefore, the good accuracy of the model to predict the experimental results supports the validity of the hypothesis used to build the model:

- All the conduction information is gathered into the assumption of infinite series-parallel association of particles. Therefore, the effective *g* factor in a compacted panel is as low as 0.33, which means that the solid conduction can be reduced 2.7 times regarding the bulk material.
- There is a coupling effect that is responsible for the highest contribution to the total thermal conductivity at ambient pressure.

Note that the model is developed in a certain range of densities (160–360 kg/m^3), cell sizes (400–3200 nm), pressures (0.02–1013 mbar), and temperatures (10–40 °C). Therefore, it is, at least, valid for compacted panels made by micronized micro-and nanocellular PMMA in that range but can also be valid for other micronized cellular polymers or systems consisting of particles in contact. As previously commented, for different materials, the different inherent parameters (conduction of the solid, *f* factor, and extinction coefficient) may be determined to extend the model. Finally, possible discrepancies between predictions and experimental data may be due to the open cell content and/or the use of the mean values of the different parameters for the calculations.

In the next section, the equations developed in the model are going to be used to extrapolate the behavior to densities and cell sizes out of the range of study of this work.

4.2. Effect of the cell size, particle size, pressure, and density on the thermal conductivity

The model can be used to predict trends and study the effect of the different parameters on the thermal conductivity of compacted panels. On the one hand, **Fig. 9a**, **6b**, and **c** show the effect of the particle size on the thermal conductivity at different pressures. The predictions were calculated at 10 °C, assuming 500 nm of cell size and an apparent density of 150 kg/m^3 (Fig. 9a), 100 kg/m^3 (Fig. 9b), and 50 kg/m^3 (Fig. 9c). Note that since the particle size is not in the nanoscale it does not affect the total thermal conductivity at ambient pressure or at maximum vacuum, only the curve at different pressures. As the particle size is reduced the Knudsen effect occurs at higher pressures (requiring a lower vacuum to fully evacuate the material), so for applications like vacuum insulation panels the smaller the particle size the better. Furthermore, it is observed that as density decreases from 150 kg/m^3 to 100 kg/m^3 the total thermal conductivity decreases, but at 50 kg/m^3 it increases again. When density decreases the conduction through the solid phase and the coupling decrease, whereas the conduction through the cells phase and the radiation increase (Eq. (9)), leading to a compromise between the heat transfer mechanisms that result in an optimum density. On the other hand, **Fig. 9d**, **6e**, and **f** show the effect of the cell size on the thermal conductivity at different pressures for a fixed particle size of 100 μm. The predictions were performed at 10 °C, assuming an apparent density of 150 kg/m^3 (Fig. 9d), 100 kg/m^3 (Fig. 9e), and 50 kg/m^3 (Fig. 9f). In this case, the cell size is affecting both the conduction through the cells phase and the radiation. Regarding the radiation, the lower the cell size the higher the radiation since the material becomes transparent to infrared radiation [15,33,34], obtaining higher thermal conductivities. Also, when the density is reduced there is less amount of matter to absorb/scatter the thermal radiation, so the radiation rises hugely. This effect can be easily observed at vacuum. With respect to the conduction through the cells phase, it is observed that the first fall of the thermal conductivity as the pressure is reduced is less sharp when the cell size is reduced due to the Knudsen effect. These predictions show that for the compacted panels micrometric cells are promising candidates for this application in VIP panels. However, reaching smaller particle sizes would be more challenging as the cell size increases.

Fig. 10 shows the effect of the contributions of each transfer mechanism on the thermal conductivity at different pressures. The predictions were performed at 10 °C, assuming 500 nm of cell size, 100 μm of particle size, and an apparent density of 150 kg/m^3 (**Fig. 10a** and **6d**), 100 kg/m^3 (**Fig. 10b** and **6e**), and 50 kg/m^3 (**Fig. 10c** and **6f**). On the one hand, it is observed that since the conduction through the solid phase does not depend on the cell size or the particle size its contribution is constant and becomes more important under vacuum. As density reduces the conduction through the solid phase decreases. On the other hand, radiation depends on the cell size and on the relative density. For a given combination of density and cell size, its contribution is also constant and becomes more important under vacuum. As previously

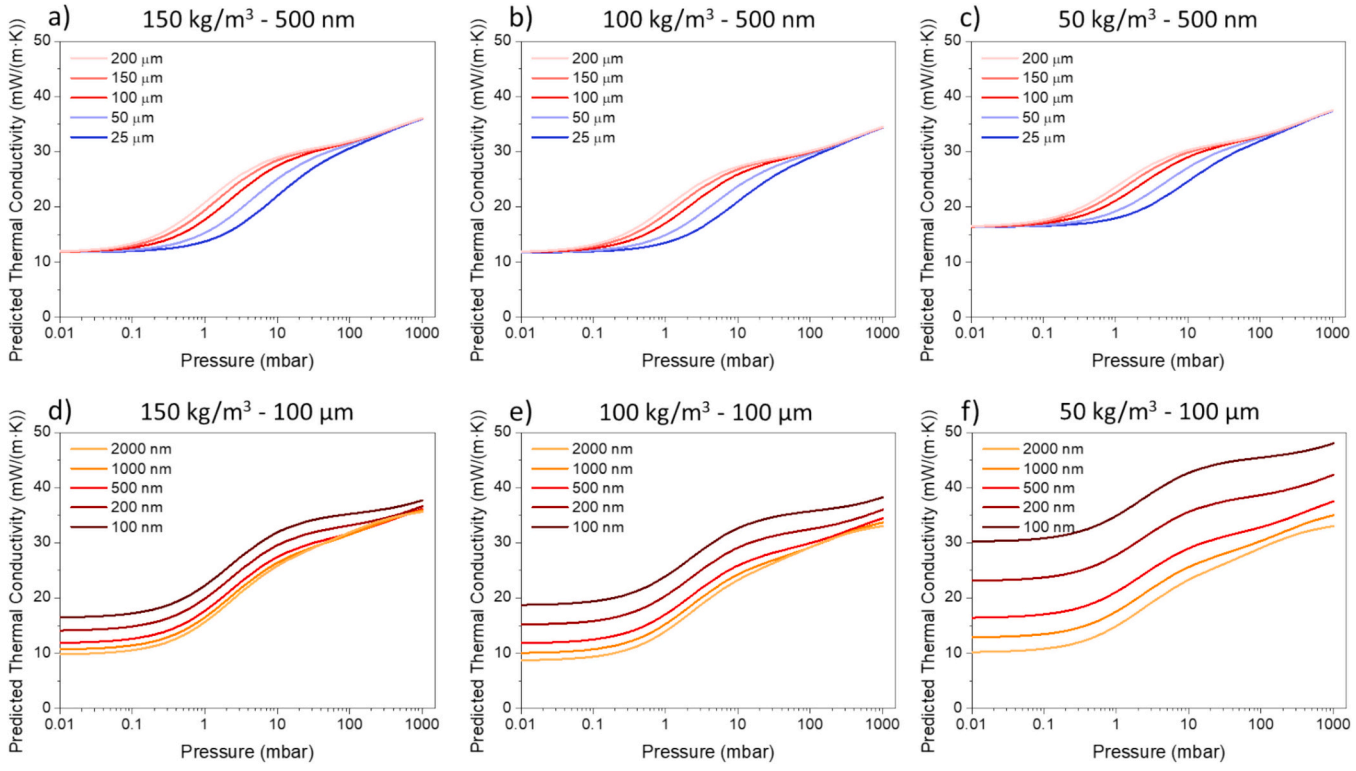

Fig. 9. Effect of the particle size on the thermal conductivity at different pressures. Predictions were performed at 10 °C, assuming 500 nm of cell size and an apparent density of 150 kg/m^3 (a), 100 kg/m^3 (b), and 50 kg/m^3 (c). b) Effect of the cell size on the thermal conductivity at different pressures. Predictions were performed at 10 °C, assuming 100 μm of particle size and an apparent density of 150 kg/m^3 (d), 100 kg/m^3 (e), and 50 kg/m^3 (f).

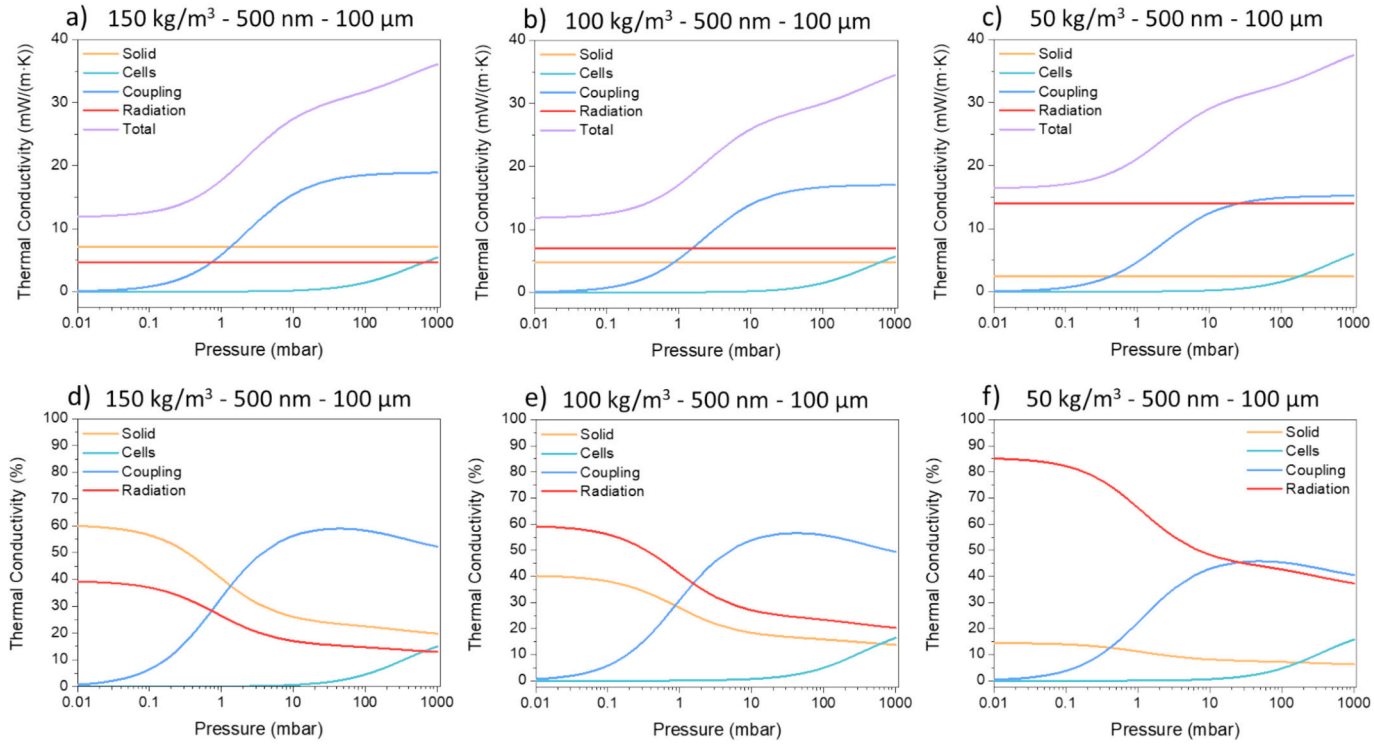

Fig. 10. Predicted contribution at 10 °C of each transfer mechanism to the total thermal conductivity in mW/(m·K) assuming 500 nm of cell size, 100 µm of particle size and density of 150 kg/m^3 (a), 100 kg/m^3 (b), and 50 kg/m^3 (c). Predicted contribution at 10 °C of each transfer mechanism to the total thermal conductivity in % of the total thermal assuming 500 nm of cell size, 100 µm of particle size, and density of 150 kg/m^3 (d), 100 kg/m^3 (e), and 50 kg/m^3 (f).

commented, as density decreases the amount of matter to absorb/scatter the thermal radiation is reduced, so the radiation rises hugely as observed in **Fig. 10a**, **7b**, and **c**. Therefore, at vacuum for very low-density materials, most of the thermal conductivity is due to the radiation contribution (Fig. 10f). Meanwhile, conduction through the gas phase depends on the density and the cell size. Since the cell size is much smaller than the particle size, the contribution of the conduction through the gas becomes null at higher pressures. Finally, the coupling depends on the density and the particle size. It is noticed that as density increases contribution of the coupling effect rises, being higher than 50 % of the total thermal conductivity for pressures higher than 5 mbar for materials with densities higher than 100 kg/m^3 (**Fig. 10d** and **7e**).

In Fig. 11 maps of thermal conductivity as a function of the cell size and the relative density are presented, assuming 10 °C of temperature. **Fig. 11a** and **8c** show the thermal conductivity of the bulk samples at ambient pressure and at vacuum, respectively, whereas **Fig. 11b** and **8d** show the thermal conductivity of the compacted panels at ambient pressure and at vacuum, respectively. For the compacted panels, a particle size of 100 µm has been assumed.

Regarding the predictions, the compacted panels present lower thermal conductivity due to their discontinuous cellular structure. At ambient pressure, a minimum (thermal conductivities between 30.0 and 32.5 mW/(m·K)) appear in the region of around 70 kg/m^3 (relative densities of 0.06) and cell sizes higher than 1600 nm for the compacted panels (Fig. 11b). This minimum is like the one obtained for the bulk material in that region and may be due to the increase in the radiation contribution when the solid volume fraction (which absorbs the radiation) is reduced (Fig. 11a). However, in the bulk materials, a second region with minimum thermal conductivity was obtained for cell sizes in the nanoscale, whereas this does not appear in the panels. This can be due to the fact that this model assumes a small relevance of the gas inside the cells, so the presence of nanometric cells is not enough to assure a good insulation performance. Meanwhile, at vacuum, the compacted panels (Fig. 11d) also present lower thermal conductivity than the bulk materials (Fig. 11c). For powdered systems based on nanocellular polymers, thermal conductivities higher than 10 mW/(m·K) are predicted, while bulk materials are limited to values over 15 mW/mK. This minimum is again obtained for cell sizes of around 2–3 µm as already discussed in Fig. 9. Then, microcellular polymers can be suitable for this application as long as the cell size is small enough to assure a good micronization of the material.

In the previous graphs, a solid structure factor of 0.89 has been assumed for the nanocellular polymer (effective solid structure factor of 0.33 for the micronized materials). However, for low-density foams, g factors of 0.3–0.6 are usually reported [20,21,65]. To account for the possible configurations of nanocellular polymers that could lead to reduced solid structure factors, Fig. 12 shows a map of the thermal conductivity of compacted panels (100 µm of particle size) as a function of the cell size and the relative density assuming 10 °C of temperature at ambient pressure (first raw) and at vacuum (second raw) but using different solid structural factors $g = 0.7$ (**Fig. 12a** and **9d**), $g = 0.5$ (**Fig. 12b** and **9e**), and $g = 0.3$ (**Fig. 12c** and **9f**) (effective solid structure factors of 0.26, 0.18, and 0.11, respectively). It is observed that as the solid structure factor decreases, the minimum thermal conductivity that can be reached is reduced. Thus, the reduction of g from 0.89 to 0.3 leads to a reduction of 2 mW/(m·K) in compacted panels (from 30 to 28 mW/(m·K)) at ambient pressure. Meanwhile, at vacuum thermal conductivities as low as 4 mW/(m·K) can be obtained (Fig. 12f).

Finally, it is important to recall that the present model does not take into account that the contact points between particles may act as radiation scatter points, which may reduce further the radiation, improving the thermal insulation of these materials. Furthermore, radiation can be reduced by introducing particles that absorb or scatter infrared radiation. Therefore, compacted panels are a new promising eco-friendly, and low-cost alternative materials for the generation of VIP cores.

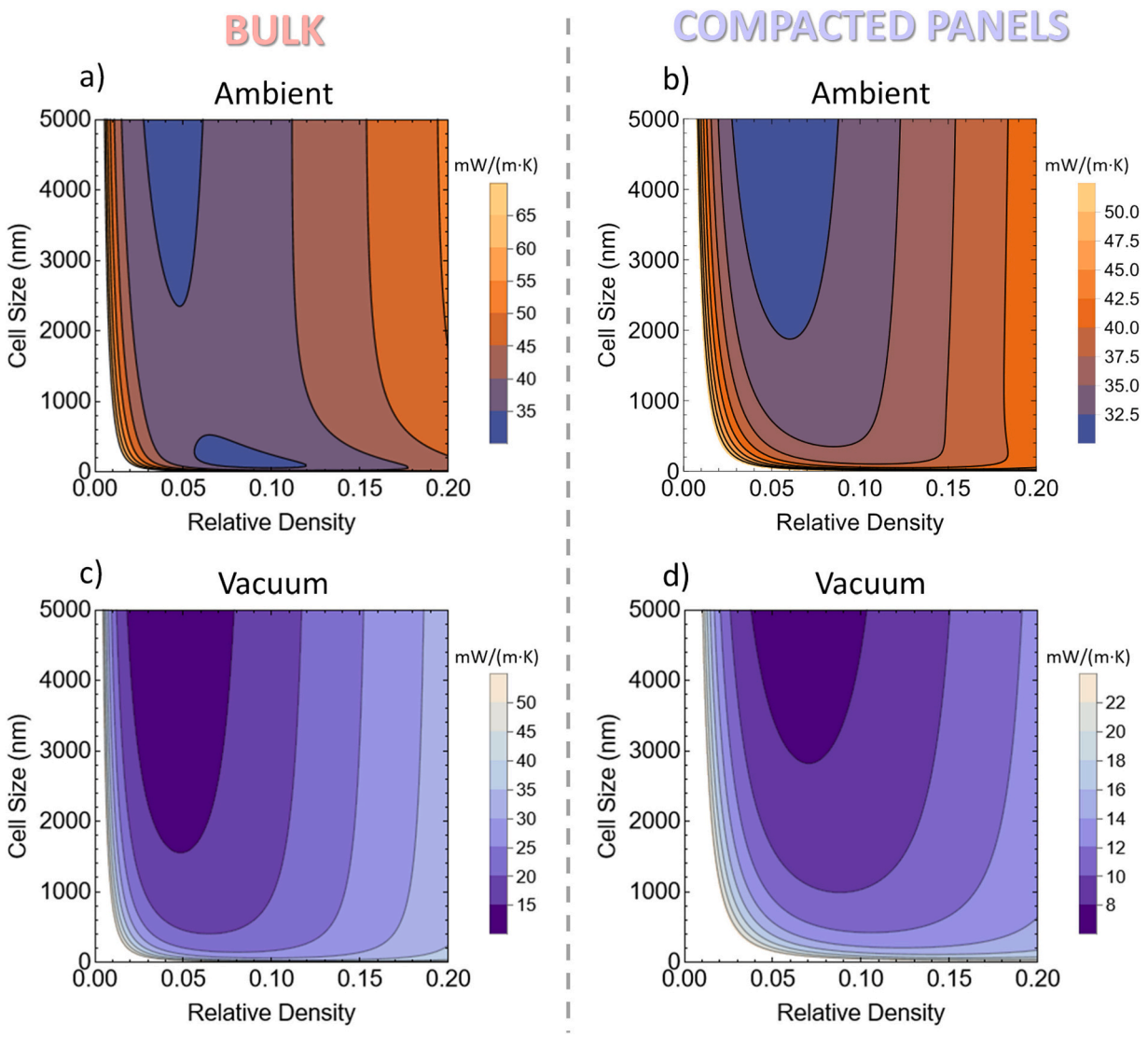

Fig. 11. Predictions of thermal conductivity as a function of the cell size and the relative density assuming 10 °C of temperature based on [15] for the bulk materials and on Eq. (9) for the compacted panels: a) bulk at ambient pressure, b) compacted panels at ambient pressure, c) bulk at vacuum, and d) compacted panels at vacuum. For the compacted panels, a particle size of 100 μm was assumed.

5. Conclusions

In this work, a model to predict the thermal conductivity of compacted panels based on micronized microcellular and nanocellular PMMA is established. The model is unique in introducing the concept of infinite association of resistances for quantifying the conduction through the powder particles. In addition, a new heat transfer mechanism (the coupling effect), never observed in bulk nanocellular polymers, appears due to the discontinuous solid phase and the model is able to quantify this mechanism. Thus, a semi-empirical model able to predict the thermal conductivity of compacted materials based on microcellular and nanocellular PMMA was developed. The semi-empirical model depends only on the properties of the compacted material (apparent relative density, cell size, and particle size) and the measurement conditions (temperature and pressure). The model presents high accuracy for the compacted panels at ambient pressure, at maximum vacuum, and also at different vacuum pressures. The model also allows analyzing the contribution of each heat transfer mechanism, showing that the contribution of the coupling effect is higher than 50 % of the total thermal contribution for pressures higher than 5 mbar. For nanocellular polymers (at 10 °C), the model predicts minimum thermal conductivities of 32.5 mW/(m·K) at ambient pressure and of 10 mW/(m·K) at maximum vacuum. Furthermore, depending on the solid structure configuration, the model predicts thermal conductivities as low as 4 mW/(m·K) at maximum vacuum. These results make the compacted panels based on micronized microcellular and nanocellular polymers potential candidates to be used as alternative materials for VIP productions. Finally, this works helps to identify the strengths and weaknesses of these materials and how they could be further improved in the future. The particle size was found to be an important parameter, while the radiation term played an important role. Thus, this paper paves the way for further studies in reducing the particle size and adding infrared blockers, which would for sure boost the performance of these new materials.

CRediT authorship contribution statement

Ismael Sánchez-Calderón: Writing – original draft, Methodology, Investigation, Formal analysis, Conceptualization. **Félix Lizalde-Arroyo:** Investigation. **Judith Martín-de-León:** Conceptualization. **Miguel Ángel Rodríguez-Pérez:** Writing – review & editing, Supervision, Funding acquisition, Conceptualization. **Victoria Bernardo:**

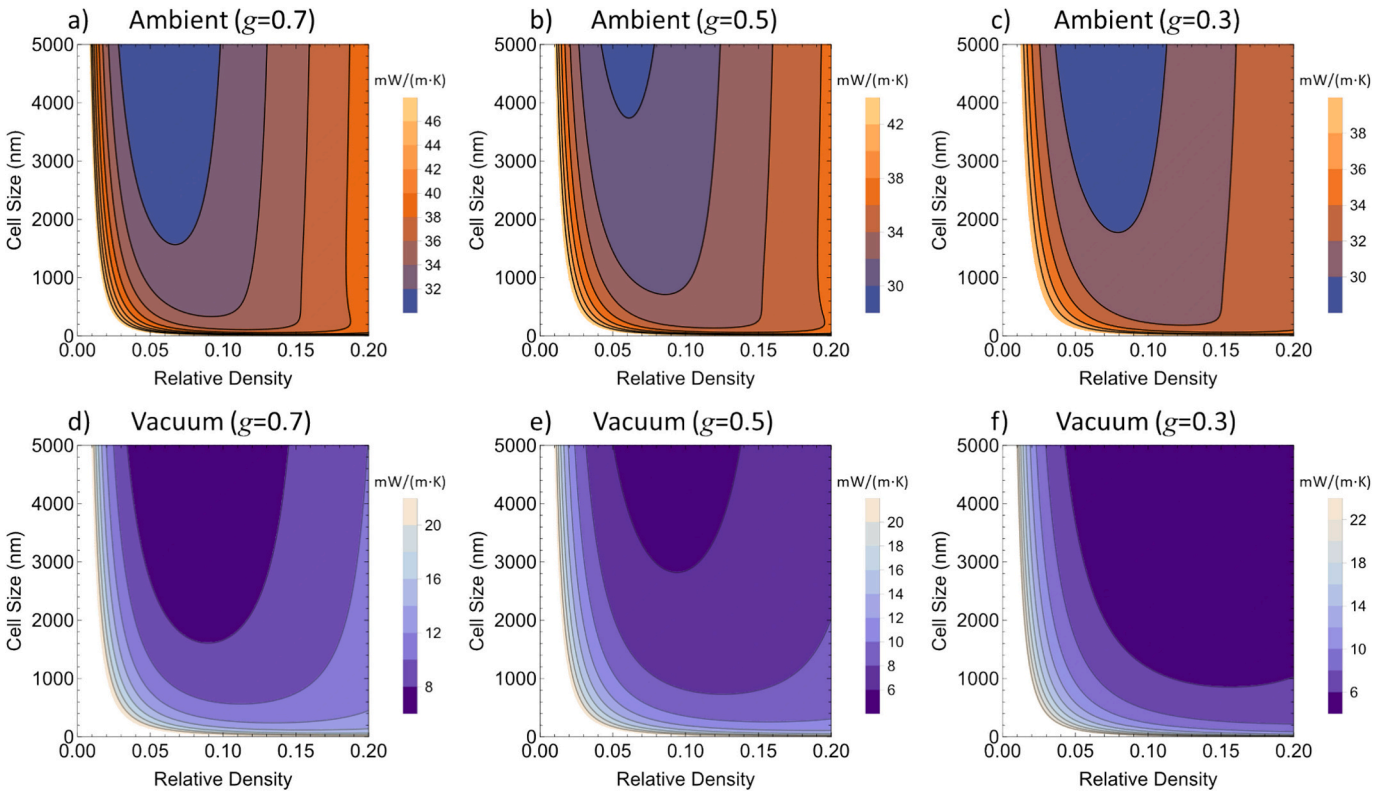

Fig. 12. Map of thermal conductivity of compacted panels as a function of the cell size and the relative density assuming 10 °C of temperature and ambient pressure (first row) and under vacuum (second row) using different structure factors: $g = 0.7$ (a-d), $g = 0.5$ (b-e), and $g = 0.3$ (c-f).

Writing – review & editing, Supervision, Conceptualization.

Declaration of competing interest

The authors declare that they have no known competing financial interests or personal relationships that could have appeared to influence the work reported in this paper.

Acknowledgments

Financial assistance from the Junta of Castile and Leon grant (I. Sánchez-Calderón and VA202P20) is gratefully acknowledged. Financial support from the Spanish Ministry of Science, Innovation, and Universities (RTI2018-098749-B-I00, PID2021-127108OB-I00, TED2021-130965B-I00, PDC2022-133391-I00, and PTQ2019-010560 (Victoria Bernardo-García)) is gratefully acknowledged. Financial support from the European Regional Development Fund of the European Union and the of Castile and Leon ((ICE): R&D PROJECTS IN SMEs: PAVIPEX. 04/18/VA/008 and M-ERA.NET PROJECT: FICACEL. 11/20/VA/0001) is gratefully acknowledged. This work was supported by the Regional Government of Castilla y León (Junta de Castilla y León), by the Ministry of Science and Innovation MICIN, and the European Union NextGenerationEU/PRTR.

Data availability

Data will be made available on request.

References

[1] R. Baetens, B.P. Jelle, J.V. Thue, M.J. Tenpierik, S. Grynning, S. Uvsløkk, A. Gustavsen, Vacuum insulation panels for building applications: a review and beyond, Energ. Build. 42 (2010) 147–172, https://doi.org/10.1016/j.enbuild.2009.09.005.

[2] W. Villasmil, L.J. Fischer, J. Worlitschek, A review and evaluation of thermal insulation materials and methods for thermal energy storage systems, Renew. Sust. Energ. Rev. 103 (2019) 71–84, https://doi.org/10.1016/j.rser.2018.12.040.

[3] M. Casini, Smart Buildings, 2016th ed., Elsevier, 2016 https://doi.org/10.1016/C2015-0-00182-4.

[4] S. Schiavoni, F. D'Alessandro, F. Bianchi, F. Asdrubali, Insulation materials for the building sector: a review and comparative analysis, Renew. Sust. Energ. Rev. 62 (2016) 988–1011, https://doi.org/10.1016/j.rser.2016.05.045.

[5] M. Casini, Advanced construction materials, in: Constr. 4.0, Elsevier, 2022, pp. 337–404, https://doi.org/10.1016/B978-0-12-821797-9.00005-2.

[6] S.E. Kalnæs, B.P. Jelle, Vacuum insulation panel products: a state-of-the-art review and future research pathways, Appl. Energy 116 (2014) 355–375, https://doi.org/10.1016/j.apenergy.2013.11.032.

[7] S. Fantucci, A. Lorenzati, A. Capozzoli, M. Perino, Analysis of the temperature dependence of the thermal conductivity in vacuum insulation panels, Energ. Build. 183 (2019) 64–74, https://doi.org/10.1016/j.enbuild.2018.10.002.

[8] T. Beikircher, M. Demharter, Heat transport in evacuated perlite powders for super-insulated long-term storages up to 300 °C, J. Heat Transf. 135 (2013) 1–11, https://doi.org/10.1115/1.4023351.

[9] G. Reichenauer, U. Heinemann, H.P. Ebert, Relationship between pore size and the gas pressure dependence of the gaseous thermal conductivity, Colloids Surfaces A Physicochem. Eng. Asp. 300 (2007) 204–210, https://doi.org/10.1016/j.colsurfa.2007.01.020.

[10] J. Fricke, H. Schwab, U. Heinemann, Vacuum insulation panels – exciting thermal properties and Most challenging applications, Int. J. Thermophys. 27 (2006) 1123–1139, https://doi.org/10.1007/s10765-006-0106-6.

[11] M. Bouquerel, T. Duforestel, D. Baillis, G. Rusaouen, Heat transfer modeling in vacuum insulation panels containing nanoporous silicas - a review, Energ. Build. 54 (2012) 320–336, https://doi.org/10.1016/j.enbuild.2012.07.034.

[12] Á. Szabó, Á. Lakatos, Thermal analysis of aerogels and their vacuum-formed forms, their potential uses, and their effects on the environment, Case Stud. Therm. Eng. 56 (2024) 104284, https://doi.org/10.1016/j.csite.2024.104284.

[13] Á. Lakatos, E. Lucchi, Thermal performances of super insulation materials (SIMs): a comprehensive analysis of characteristics, heat transfer mechanisms, laboratory tests, and experimental comparisons, Int. Commun. Heat Mass Transf. 152 (2024) 107293, https://doi.org/10.1016/j.icheatmasstransfer.2024.107293.

[14] Á. Lakatos, M. Csontos, A. Csík, Investigation of both thermal parameters and applications of closed-cell plastic thermal insulation foams with building energetic aspects, J. Therm. Anal. Calorim. 149 (2024) 11171–11182, https://doi.org/10.1007/s10973-023-12789-8.

[15] I. Sánchez-Calderón, V. Bernardo, J. Martín-de-León, M.Á. Rodríguez-Pérez, Thermal conductivity of low-density micro-and nanocellular poly(methyl-methacrylate) (PMMA): experimental and modeling, Mater. Des. 221 (2022) 110938, https://doi.org/10.1016/j.matdes.2022.110938.

[16] S. Sonnick, M. Meier, J. Ross-Jones, L. Erlbeck, I. Medina, H. Nirschl, M. Rädle, Correlation of pore size distribution with thermal conductivity of precipitated silica and experimental determination of the coupling effect, Appl. Therm. Eng. 150 (2019) 1037–1045, https://doi.org/10.1016/j.applthermaleng.2019.01.074.
[17] K. Swimm, S. Vidi, G. Reichenauer, H.P. Ebert, Coupling of gaseous and solid thermal conduction in porous solids, J. Non-Cryst. Solids 456 (2017) 114–124, https://doi.org/10.1016/j.jnoncrysol.2016.11.012.
[18] H. Ebert, Thermal Properties of Aerogels, Aerogels Handb, in, 2011, pp. 537–564, https://doi.org/10.1007/978-1-4419-7589-8.
[19] M. Alvarez-Lainez, M.A. Rodriguez-Perez, J.A. De Saja, Thermal conductivity of open-cell polyolefin foams, J. Polym. Sci. Part B Polym. Phys. 46 (2008) 212–221.
[20] P.G. Collishaw, J.R.G. Evans, An assessment of expressions for the apparent thermal conductivity of cellular materials, J. Mater. Sci. 29 (1994) 486–498, https://doi.org/10.1007/BF01162512.
[21] N.C. Hilyard, A. Cunningham, Low Density Cellular Plastics Physical Basis of Behaviour, 1994, https://doi.org/10.1007/978-94-011-1256-7.
[22] H. Jeffreys, Some cases of instability in fluid motion, Proc. R. Soc. London. Ser. A, Contain. Pap. a Math. Phys. Character. 118 (1928) 195–208, https://doi.org/10.1098/rspa.1928.0045.
[23] K. Swimm, G. Reichenauer, S. Vidi, H.P. Ebert, Impact of thermal coupling effects on the effective thermal conductivity of aerogels, J. Sol-Gel Sci. Technol. 84 (2017) 466–474, https://doi.org/10.1007/s10971-017-4437-5.
[24] K. Swimm, G. Reichenauer, S. Vidi, H.-P. Ebert, Gas pressure dependence of the heat transport in porous solids with pores smaller than 10 μm, Int. J. Thermophys. 30 (2009) 1329–1342, https://doi.org/10.1007/s10765-009-0617-z.
[25] J.-J. Zhao, Y.-Y. Duan, X.-D. Wang, B.-X. Wang, Effects of solid–gas coupling and pore and particle microstructures on the effective gaseous thermal conductivity in aerogels, J. Nanopart. Res. 14 (2012) 1024, https://doi.org/10.1007/s11051-012-1024-0.
[26] C. Bi, G.H. Tang, Z.J. Hu, Heat conduction modeling in 3-D ordered structures for prediction of aerogel thermal conductivity, Int. J. Heat Mass Transf. 73 (2014) 103–109, https://doi.org/10.1016/j.ijheatmasstransfer.2014.01.058.
[27] S. Verma, H. Singh, Predicting the conductive heat transfer through evacuated perlite based vacuum insulation panels, Int. J. Therm. Sci. 171 (2022) 107245, https://doi.org/10.1016/j.ijthermalsci.2021.107245.
[28] J. Liu, P. Buahom, C. Lu, H. Yu, C.B. Park, Microscopic revelation of the solid–gas coupling and Knudsen effect on the thermal conductivity of silica aerogel with inter-connected pores, Sci. Rep. 12 (2022) 21034, https://doi.org/10.1038/s41598-022-24133-5.
[29] I. Sánchez-Calderón, V. Bernardo, F. Lizalde-Arroyo, J. Martín-de-León, M.Á. Rodríguez-Pérez, Development of new vacuum insulation core panels using micronized nanocellular poly(methyl-methacrylate) (PMMA), Appl. Mater. Today 41 (2024) 102483, https://doi.org/10.1016/j.apmt.2024.102483.
[30] H. Yu, H. Zhang, J. Zhao, J. Liu, X. Xia, X. Wu, Thermal conductivity of micro/nano-porous polymers: prediction models and applications, Front. Phys. 17 (2021), https://doi.org/10.1007/s11467-021-1107-4.
[31] C. Forest, P. Chaumont, P. Cassagnau, B. Swoboda, P. Sonntag, Polymer nano-foams for insulating applications prepared from CO2 foaming, Prog. Polym. Sci. 41 (2015) 122–145, https://doi.org/10.1016/j.progpolymsci.2014.07.001.
[32] G. Wang, C. Wang, J. Zhao, G. Wang, C.B. Park, G. Zhao, Modelling of thermal transport through a nanocellular polymer foam: toward the generation of a new superinsulating material, Nanoscale 9 (2017) 5996–6009, https://doi.org/10.1039/c7nr00327g.
[33] V. Bernardo, J. Martin-de Leon, J. Pinto, U. Schade, M.A. Rodriguez-Perez, On the interaction of infrared radiation and nanocellular polymers: first experimental determination of the extinction coefficient, Colloids Surfaces A Physicochem. Eng. Asp. 600 (2020), https://doi.org/10.1016/j.colsurfa.2020.124937.
[34] P. Buahom, C. Wang, M. Alshrah, G. Wang, P. Gong, M. Tran, C.B. Park, Wrong expectation of superinsulation behavior from largely-expanded nanocellular foams, Nanoscale (2020), https://doi.org/10.1039/d0nr01927e.
[35] V. Bernardo, J. Martin-de Leon, J. Pinto, R. Verdejo, M.A. Rodriguez-Perez, Modeling the heat transfer by conduction of nanocellular polymers with bimodal cellular structures, Polymer (Guildf) 160 (2019) 126–137, https://doi.org/10.1016/j.polymer.2018.11.047.
[36] S.S. Sundarram, W. Li, On thermal conductivity of micro- and nanocellular polymer foams, Polym. Eng. Sci. 53 (2013) 1901–1909, https://doi.org/10.1002/pen.23452.
[37] I. Sánchez-Calderón, V. Bernardo, D. Cuadra-Rodríguez, J. Martín-de-León, M.Á. Rodríguez-Pérez, Micronization as a solution for enhancing the thermal insulation of nanocellular poly(methyl-methacrylate) (PMMA), Polymer (Guildf) 261 (2022) 125397, https://doi.org/10.1016/j.polymer.2022.125397.
[38] UNE-EN 1602, Thermal insulating products for building applications. Determination of the apparent density, 2013 (n.d.).
[39] J. Pinto, E. Solórzano, M.A. Rodriguez-Perez, J.A. de Saja, Characterization of the cellular structure based on user-interactive image analysis procedures, J. Cell. Plast. 49 (2013) 555–575, https://doi.org/10.1177/0021955X13503847.
[40] http://www.cellmattechnologies.com/en/software-and-methodology-for-the-characterization-of-cellular-structures/ (n.d.).
[41] ISO 4590, 2016 Rigid cellular plastics — Determination of the volume percentage of open cells and of closed cells, 2016.
[42] ASTM, C518 Standard Test Method for Steady-State Thermal Transmission Properties by Means of the Heat Flow Meter Apparatus, 2017.
[43] ISO 8301, Thermal insulation - Determination of steady-state thermal resistance and related properties - Heat flow meter, 1991.
[44] F. Almeida, H. Beyrichen, N. Dodamani, R. Caps, A. Müller, R. Oberhoffer, Thermal conductivity analysis of a new sub-micron sized polystyrene foam, J. Cell. Plast. 57 (2021) 493–515, https://doi.org/10.1177/0021955X20943101.
[45] M. Alam, H. Singh, S. Brunner, C. Naziris, Experimental characterisation and evaluation of the thermo-physical properties of expanded perlite—Fumed silica composite for effective vacuum insulation panel (VIP) core, Energ. Build. 69 (2014) 442–450, https://doi.org/10.1016/j.enbuild.2013.11.027.
[46] J.H. Kim, F.E. Boafo, S.M. Kim, J.T. Kim, Aging performance evaluation of vacuum insulation panel (VIP), Case Stud. Constr. Mater. 7 (2017) 329–335, https://doi.org/10.1016/j.cscm.2017.09.003.
[47] https://www.beforethebang.org/post/the-infinite-resistance-problem (n.d.).
[48] S. Masamune, J.M. Smith, Thermal conductivity of beds of spherical particles, Ind. Eng. Chem. Fundam. 2 (1963) 136–143, https://doi.org/10.1021/i160006a009.
[49] R.G. Deissler, C.S. Eian, Investigation of Effective Thermal Conductivities of Powders, 1952.
[50] C.T. Hsu, P. Cheng, K.W. Wong, Modified Zehner-Schlunder models for stagnant thermal conductivity of porous media, Int. J. Heat Mass Transf. 37 (1994) 2751–2759, https://doi.org/10.1016/0017-9310(94)90392-1.
[51] P. Zehner, E.U. Schlünder, Warmeleitfahigkeit von Schuttungen bei mässigen Temperaturen, Chem. Ing. Tech. 42 (1970) 933–941.
[52] W. Dai, D. Hanaor, Y. Gan, The effects of packing structure on the effective thermal conductivity of granular media: a grain scale investigation, Int. J. Therm. Sci. 142 (2019) 266–279, https://doi.org/10.1016/j.ijthermalsci.2019.04.028.
[53] J.S. Kwon, C.H. Jang, H. Jung, T.H. Song, Effective thermal conductivity of various filling materials for vacuum insulation panels, Int. J. Heat Mass Transf. 52 (2009) 5525–5532, https://doi.org/10.1016/j.ijheatmasstransfer.2009.06.029.
[54] L. Jin, J. Park, C. Lee, S. Jeong, Prediction of the effective thermal conductivity of powder insulation, Phys. Procedia 67 (2015) 970–975, https://doi.org/10.1016/j.phpro.2015.06.164.
[55] M.S. Khader, R.A. Crane, R.I. Vachon, Thermal Conductivity of Granular Materials - a Review, Pergamon Press Ltd., 1977, https://doi.org/10.1016/b978-0-08-024235-4.50014-1.
[56] C.T. Hsu, A closure model for transient heat conduction in porous media, J. Heat Transf. 121 (1999) 723–739, https://doi.org/10.1115/1.2826043.
[57] S.S. Sih, J.W. Barlow, The prediction of the thermal conductivity of powders, Proc. Solid Free. Fabr. Symp. (1994) 397–401.
[58] B. Notario, J. Pinto, E. Solorzano, J.A. de Saja, M. Dumon, M.A. Rodríguez-Pérez, Experimental validation of the Knudsen effect in nanocellular polymeric foams, Polymer (Guildf) 56 (2015) 57–67, https://doi.org/10.1016/j.polymer.2014.10.006.
[59] S. Sonnick, L. Erlbeck, M. Meier, H. Nirschl, M. Rädle, Methodical selection of thermal conductivity models for porous silica-based media with variation of gas type and pressure, Int. J. Heat Mass Transf. 187 (2022), https://doi.org/10.1016/j.ijheatmasstransfer.2022.122519.
[60] Z.-Y. Li, C.-Y. Zhu, X.-P. Zhao, A theoretical and numerical study on the gas-contributed thermal conductivity in aerogel, Int. J. Heat Mass Transf. 108 (2017) 1982–1990, https://doi.org/10.1016/j.ijheatmasstransfer.2017.01.051.
[61] Y.A. Cengel, A.J. Ghajar, Heat and Mass Transfer: Fundamentals & Applications Appendix 1, Fifth Edit, Mc Graw Hill Education, 2006.
[62] R. Siegel, J.R. Howell, Thermal Radiation Heat Transfer, Taylor & Francis, London, 1992.
[63] R.A. Campo-Arnáiz, M.A. Rodríguez-Pérez, B. Calvo, J.A. De Saja, Extinction coefficient of polyolefin foams, J. Polym. Sci. Part B Polym. Phys. 43 (2005) 1608–1617, https://doi.org/10.1002/polb.20435.
[64] U. Heinemann, J. Hetfleisch, R. Caps, J. Kuhn, J. Fricke, Evacuable guarded hot plate for thermal conductivity measurements between-200°C and 800°C, in: Adv. Therm. Insul. Proc. Eurotherm Semin. No.44At Rio Tinto - Port, 1995.
[65] J.A. Reglero Ruiz, C. Saiz-Arroyo, M. Dumon, M.A. Rodríguez-Perez, L. Gonzalez, Production, cellular structure and thermal conductivity of microcellular (methyl methacrylate)-(butyl acrylate)-(methyl methacrylate) triblock copolymers, Polym. Int. 60 (2011) 146–152, https://doi.org/10.1002/pi.2931.